



**HAL**  
open science

# Light: A new handle to control the structure of cesium lead iodide

Charles Paillard, Laurent Bellaïche

► **To cite this version:**

Charles Paillard, Laurent Bellaïche. Light: A new handle to control the structure of cesium lead iodide. *Physical Review B*, 2023, 107 (5), pp.054107. 10.1103/PhysRevB.107.054107 . hal-03993958

**HAL Id: hal-03993958**

**<https://centralesupelec.hal.science/hal-03993958>**

Submitted on 17 Feb 2023

**HAL** is a multi-disciplinary open access archive for the deposit and dissemination of scientific research documents, whether they are published or not. The documents may come from teaching and research institutions in France or abroad, or from public or private research centers.

L'archive ouverte pluridisciplinaire **HAL**, est destinée au dépôt et à la diffusion de documents scientifiques de niveau recherche, publiés ou non, émanant des établissements d'enseignement et de recherche français ou étrangers, des laboratoires publics ou privés.

# Light, a new handle to control the structure of cesium lead iodide

Charles Paillard<sup>1,\*</sup> and Laurent Bellaïche<sup>2</sup>

<sup>1</sup>*Université Paris-Saclay, CentraleSupélec, CNRS,  
Laboratoire SPMS, 91190, Gif-sur-Yvette, France.*

<sup>2</sup>*Department of Physics and Institute for Nanosciences,  
University of Arkansas, Fayetteville AR 72701, USA*

(Dated: January 10, 2023)

CsPbI<sub>3</sub> is of high interest for photovoltaic applications owing to its low bandgap, provided it could be stabilized in its  $\gamma$  perovskite phase. Instead, it energetically prefers to adopt a so-called yellow,  $\delta$  phase, with much larger bandgap and reduced photovoltaic properties. Here, using an original constrained Density Functional Theory method, we mimic the effect of thermalized photo-excited carriers, and show that larger concentrations in photo-excited carriers (i.e. larger optical pump fluences) effectively reduce the energy difference between the  $\delta$  non-perovskite ground state and the  $\gamma$  perovskite phase. Even further, the stability of the phases could be potentially reversed and therefore the  $\gamma$  phase stabilized under strong illumination. We also report large photostriction, i.e., large photo-induced strain for all phases in this material, making CsPbI<sub>3</sub> suitable for other applications such as photo-driven relays and photoactuators.

## I. INTRODUCTION

Halide perovskites represent a new hope to achieve efficient and affordable solar power conversion. They have quickly grown to achieve more than 25% power conversion efficiency [1]. Their domain of application extends far beyond the mere solar cell, as their good photo- or electroluminescent properties [2, 3] make them prime candidates for laser or light-emitting diode applications [4, 5]. However, many of those halide perovskites suffer from severe stability issues with respect to humidity or temperature, in particular when they are made of a hybrid of organic - inorganic cations [6]. As a result, the fully inorganic lead halide perovskites, CsPbX<sub>3</sub> (X=I, Br, Cl) have been considered most promising owing to their larger stability. [7]. Among those, CsPbBr<sub>3</sub> significantly starts absorbing at wavelengths below 550 nm (green), while CsPbCl<sub>3</sub> absorbs in the near UV spectral domain. [2] As a result, those two compounds are not particularly promising to convert efficiently the solar spectrum into useful energy.

On the other hand, the perovskite phase of CsPbI<sub>3</sub> absorbs wavelengths as high as 700 nm [2]. Unfortunately, lead cesium iodide is only metastable in a perovskite phase; the more stable  $\delta$ -phase has much worse optical absorption properties [8]. The instability of the perovskite phase has recently been elucidated to stem from rattling of the Cs ion in its coordination cage, based on X-ray diffraction measurements on single crystals from 100 K to 295 K [9]. The perovskite phase can nonetheless be stabilized by substituting some I<sup>-</sup> with Br<sup>-</sup> at the expense of degraded absorption properties [2], or metastabilized through cooling from the high-temperature phase [10]. Yet, temperature or pressure are slow, cumbersome and energy-inefficient

control parameters. Methods allowing to easily and efficiently control the appearance of the perovskite phase in CsPbI<sub>3</sub> are thus highly desirable.

In the present work, we study the relative stability of the main four phases of CsPbI<sub>3</sub>: the  $\delta$ -phase, which is the non-perovskite ground state; the  $\gamma$ -phase which is the low-energy orthorhombic perovskite phase; the  $\beta$ -phase is an intermediate tetragonal perovskite structure, while the  $\alpha$ -phase is the cubic prototypical and high-temperature perovskite. All four phases are depicted in the Supplementary Information.

Density Functional Theory (DFT) calculations are employed in an original scheme which constrains excited electrons (resp. holes) in the conduction (resp. valence) bands during the self-consistent cycle to mimic thermalized photo-excited carriers. Our results indicate that above bandgap light may help tune the relative stability of the  $\gamma$  and  $\delta$  phases. Even further, knowing that the  $\gamma$  phase is dynamically stable in dark conditions [11], our results may provide a pathway to trigger a transition to the perovskite phase without having to realize heavy and slow thermal cycles [10]. Furthermore, a large photo-induced strain is also calculated in all phases and in particular in the *stable*  $\delta$ -phase, which is of high importance to use CsPbI<sub>3</sub> in photostrictive devices [12].

## II. METHODS

In order to study the possibility of triggering a phase transition towards a perovskite phase in CsPbI<sub>3</sub>, we used the constrained-DFT scheme developed in Ref. [13] as implemented in Abinit [14–18], with a plane wave cutoff of 40 Ha. The Perdew-Burke-Ernzerhof (PBE) exchange correlation functional revised for solids (named PBESol) was employed. All calculations reported here include spin-orbit coupling (SOC). Plane Augmented Wave (PAW) pseudopotentials were regenerated for PBESol using the PBE pseudopotential parameters used

\* charles.paillard@centralesupelec.fr

78 in the Jollet-Torrent-Holzwarth (v1.1) table [19, 20] and  
 79 the AtomPAW software [21]. The discretization of the  
 80 Brillouin zone was performed using a  $\Gamma$ -centered mesh  
 81 having  $7 \times 10^{-3}$  Bohr $^{-1}$  sampling density along each recip-  
 82 rocal lattice vector direction. Self-consistent field cycles  
 83 were considered converged when the difference in forces  
 84 between two iterations was smaller than  $10^{-8}$  Ha.Bohr $^{-1}$ ;  
 85 structural relaxation was performed until the maxi-  
 86 mum calculated force laid below  $5 \times 10^{-7}$  Ha.Bohr $^{-1}$ .  
 87 Fermi-Dirac distributions with a smearing temperature of  
 88 0.004 Ha characterize the occupation of electronic states.  
 89 The lattice constants obtained in the electronic ground  
 90 state are in good agreement with lattice constants mea-  
 91 sured experimentally or calculated using the Local Den-  
 92 sity Approximation (LDA) [22, 23] (see Supplementary  
 93 Information [24]). The reciprocal space paths used for  
 94 the band structures in Figure 1 are detailed in Ref. [25]  
 95 In order to simulate photo-excitation, we constrained a  
 96 finite number  $n_{ph}$  of electrons (resp. holes) to lie in the  
 97 conduction (resp. valence) bands with a Fermi-Dirac dis-  
 98 tribution characterized by two separate quasi-Fermi lev-  
 99 els for photo-excited electrons and holes.

### 100 III. PHOTO-INDUCED PHASE TRANSITIONS

#### 101 A. Structural and electronic properties in dark

102 We start by describing the electronic and energetic  
 103 properties of CsPbI $_3$  in "dark" conditions ( $n_{ph} = 0$ ). The  
 104 band structures of the  $\delta$  and  $\gamma$  phases are depicted in Fig-  
 105 ures 1a,d. The  $\gamma$  phase (Figure 1a) has a direct bandgap  
 106 of 0.63 eV located at the  $\Gamma$  point. The electronic bandgap  
 107 of the  $\delta$  phase is indirect and 1.79 eV large. The top of  
 108 the valence band is located on the YT segment, while  
 109 the bottom of the conduction band is close to X. The  
 110 direct bandgap, depicted with black empty circles, is lo-  
 111 cated near X in reciprocal space, and is 1.80 eV large.  
 112 In Table I, we summarize the values of bandgaps for the  
 113  $\gamma$  and  $\delta$  phases, and compare with experimental and the-  
 114 oretical works. The predicted bandgaps calculated with  
 115 SOC underestimate both experimental and theoretical  
 116 values obtained without SOC, as consistent with the lit-  
 117 erature [26, 27, 32].

118 The energy of the four phases without photoexcitation  
 119 is depicted in Figure 2 (see points at  $n_{ph} = 0$ ). The  
 120 lowest-energy structure is the  $\delta$ -phase, which lies below  
 121 the  $\gamma$ -phase by roughly 80 meV/f.u. This qualitatively  
 122 differs from Ref. [22], but agrees well with experimental  
 123 observations of the  $\delta$ -phase being the most stable state.  
 124 The difference with Ref. [22] might be due to a different  
 125 exchange-correlation functional used. We note, further-  
 126 more, that the relative energies of the phases  $\delta$ ,  $\gamma$ ,  $\beta$  and  
 127  $\alpha$  agree well with the observed phase transitions upon  
 128 cooling. [8, 10, 23, 33, 34]

	$\delta$ -phase		$\gamma$ -phase
	$E_{g,indirect}$	$E_{g,direct}$	$E_{g,direct}$
This work, PBEsol, SOC	1.79	1.80	0.63
This work, PBEsol, no SOC	2.37	2.48	1.59
Ref. [28], PBE	-	-	1.78
Ref. [29], PBE	-	2.56	-
Ref. [30], PBE	-	2.6	1.75
Ref. [31], Exp	-	-	1.68
Ref. [9], Exp	-	2.58	1.63

TABLE I. Summary of electronic bandgaps, in eV, of different phases in CsPbI $_3$ .

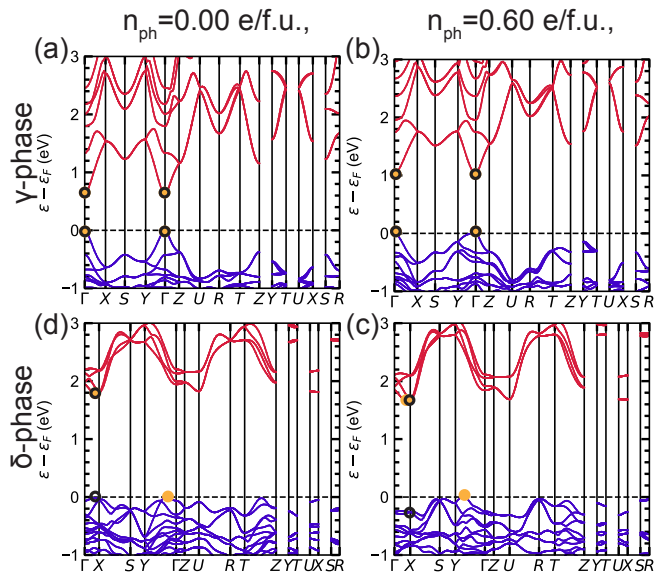


FIG. 1. Band structures obtained in the  $\gamma$  (a-b) and  $\delta$  (c-d) phases for  $n_{ph} = 0.00$  e/f.u. (electronic ground state; a and c) and  $n_{ph} = 0.6$  e/f.u. (b and d) respectively; orange plain circles indicate the location of the electronic bandgap, and black empty circles depict the direct bandgap.

#### 129 B. Energetics of phases under photoexcitation

130 Upon increasing the relative concentration of photo-  
 131 excited carriers  $n_{ph}$ , the energy difference between the  $\delta$   
 132 phase and  $\gamma$  phase (teal circles in Figure 2) significantly  
 133 decreases, and even changes sign at 0.3 e/f.u. This indi-  
 134 cates that (i) for concentrations lower than 0.3 e/f.u.,  
 135 the transition temperature between the  $\delta$  and  $\gamma$  phases  
 136 will potentially decrease when illuminating the sample  
 137 with above-bandgap light and large fluence; and (ii) a  
 138 potential phase transition from the yellow  $\delta$  phase to the  
 139 perovskite  $\gamma$  phase could occur under sufficiently intense  
 140 illumination with above bandgap energy photons. For a  
 141 thin film, such concentration is reachable with high in-  
 142 tensity lasers. Prior experiments on MAPbI $_3$  [35] and  
 143 a simple model (see Appendix A) indicate that laser  
 144 pulses of 25 mJ.cm $^{-2}$  fluence and 3 eV photon energy

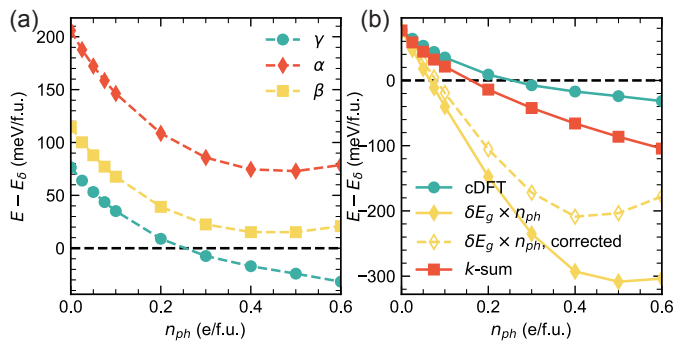


FIG. 2. (a) Energy of the  $\alpha$ ,  $\beta$ ,  $\gamma$  phases relative to the  $\delta$  phase as a function of the concentration of photo-excited carriers; (b) Comparison between the constrained-DFT calculations (teal circles), the toy model given in Eq. 1 (yellow diamonds), the toy model corrected using the experimental bandgaps (yellow dashed diamonds), and numerical integration (red squares) of the population of the "dark" band structures electronic states (see Appendix A for details.)

may achieve these large concentration of photo-excited carriers. None of the other known phases of  $\text{CsPbI}_3$  seem to become more stable in the range of concentrations in photo-excited carriers explored here.

We now attempt to elucidate the origin of this potential photo-induced phase transition. In other perovskites, mostly oxides and ferroelectrics, previous works showed that photo-excited carriers had a strong impact on phonon instabilities. [13, 36] In particular, in cubic lead titanate and barium titanate, it had been found that phonon instabilities related to the development of electrical polarization were suppressed under illumination [13]. Here, the phonon spectrum of the cubic  $\alpha$  phase (see Supplementary Information) shows that photo-excited carriers hardly modify the unstable phonon branches. This is consistent with the fact that no other perovskite-phase becomes more stable than the  $\gamma$  phase in Figure 2. There does not seem to be any other perovskite phase that could develop under illumination besides the  $\gamma$  phase, which is itself dynamically stable [11].

### C. Toy model

As a result, the case could be made that the proposed phase transition origin lies in the difference of electronic bandgaps of the  $\delta$  and  $\gamma$  phases. In a two-level system (e.g. limiting ourselves to the bottom of the valence band and top of the conduction band), a simple toy model can be designed to further prove this point. Akin to the extension of Landau's theory to the description of degenerate semiconductors [37] or to explain photostriction in ferroelectric oxides [38], one may simply say that the difference of energy between the two phases is:

$$E_\gamma(n_{ph}) - E_\delta(n_{ph}) = \Delta E_0 + \delta E_g(n_{ph}) \cdot n_{ph} \quad (1)$$

In the above equation,  $\Delta E_0$  is the energy difference between the  $\delta$  and  $\gamma$  phase in "dark" conditions (roughly 80 meV/f.u.);  $\delta E_g(n_{ph}) = E_{g,\gamma}(n_{ph}) - E_{g,\delta}(n_{ph})$  denotes the difference of bandgaps between the  $\gamma$  and  $\delta$  phases, and  $n_{ph}$  represents the concentration of photo-excited carriers. We plot that quantity in Figure 2b as filled yellow diamond, for both unclamped and clamped calculations. It can be seen that qualitatively the result of the *ab-initio* calculations and those obtained from Equation 1 are similar. This supports the scenario of an electronically controlled energy difference between the two phases. Quantitative discrepancies between the model in Equation 1 and DFT results stem from the fact that the photo-excited carriers are distributed across more than one level and one  $k$ -point owing to the finite smearing temperature. One should, in fact, integrate over the (partially) occupied conduction (and valence) states in order to obtain a better match. The integration over the ground state band structure is depicted in red squares in Fig 2b and detailed in Appendix B. The agreement is quantitatively better, and the remaining difference with constrained-DFT calculations is likely to stem from some band reconfiguration under illumination.

Note that, because our calculations underestimate the bandgap of  $\text{CsPbI}_3$ , the critical concentration of photo-excited carriers is likely underestimated. We used our toy model (see Equation 1) with experimental values of the bandgaps of the  $\gamma$  and  $\delta$  phases. The corrected curve, in dashed yellow diamonds in Figure 2b, slightly increases the critical  $n_{ph}$  of the transition. Interestingly, we also performed some calculations without SOC (see Supplementary Information [24]). In such case, the bandgaps of both the  $\delta$  and  $\gamma$  phases match the experimental ones well. The transition is then observed at a larger concentration of photo-excited carriers ( $\approx 0.6$  e/f.u.), as expected from the electronic nature of the photo-induced phase transition. The true critical concentration would be better determined using more accurate and costly exchange-correlation functionals.

Given the electronic nature of the proposed phase transition, one might wonder whether the formation of excitons could hinder the present phenomenon. Indeed, we have so far treated the photo-excited electrons and holes using a one-body Hamiltonian provided by the Kohn-Sham implementation of DFT. We note, however, that the exciton binding energy in  $\text{CsPbI}_3$  reported in magneto-optical experiments is fairly small, of the order of 15 meV [39]; likewise, calculations report values in the range 1.5-44 meV [40, 41]. In other words, and in particular at non-cryogenic temperatures, excitons will mostly dissociate into photo-excited free carriers. Note also that we need demanding numerical criteria to obtain well converged results, which is incompatible with the use of larger supercells. Consequently, the tendency of hybrid perovskites to disorder and to adopt medium range correlations [42, 43], and how these latter react to illumination, are not explored in this work. At last, we focused on phases which were previously experimentally

234 reported. It is possible, although no evidence points in  
 235 that direction, that other unknown phases could be ac-  
 236 cessed in CsPbI<sub>3</sub> under illumination. The use of genetic  
 237 algorithms coupled to the constrained-DFT method used  
 238 in this work could reveal such phases.

#### 239 IV. PHOTOSTRICTION

240 We also looked at the photostrictive response of  
 241 CsPbI<sub>3</sub>. It is given in Table II, in which estimates use the  
 242 value of the photo-induced strain at  $n_{ph} = 0.025$  e/f.u. in  
 243 Figure 3. We chose such value because it is small enough  
 244 to be in a linear regime for most phases in CsPbI<sub>3</sub>. Con-  
 245 sequently, we plot, in Figure 3, the photo-induced strain  
 246 for all four phases of CsPbI<sub>3</sub> considered in this work.  
 247  $a$ ,  $b$  and  $c$  refer to the lattice constants of the princi-  
 248 pal axes sorted by increasing length. In the case of the  
 249  $\alpha$  cubic phase for which  $a = b = c$ , we report only  $a$ ,  
 250 while for the  $\beta$  tetragonal phase,  $a = b \neq c$ , and we  
 251 report only  $a$  and  $c$ . Interestingly, and as also summa-  
 252 rized in Table II, the  $\delta$ -phase exhibits the largest pho-  
 253 tostrictive response. Compared to calculations of bulk  
 254 oxides such as BiFeO<sub>3</sub> [44], PbTiO<sub>3</sub> [38] or the brown-  
 255 millerite SrCoO<sub>2.5</sub> [45], CsPbI<sub>3</sub> exhibits superior pho-  
 256 tostrictive properties in all of its phases. Note that in  
 257 Table II, the photostriction of rhombohedral BiFeO<sub>3</sub> re-  
 258 ports that of the pseudocubic cell parameter, calculated  
 259 using the  $\Delta$ SCF method in Table 1 of Ref. [44]; similarly  
 260 for rhombohedral BaTiO<sub>3</sub> [38]. Note also that we report  
 261 in Table II, photo-induced strains from  $\Delta$ SCF calcula-  
 262 tions [38, 44, 46] corresponding to indirect transitions to  
 263 match as closely as possible the results that would be  
 264 obtained using the constrained-DFT method employed  
 265 here.

266 We must also stress that at large concentrations in  
 267 photo-excited carriers ( $n_{ph} > 0.1$  e/f.u.), the photo-  
 268 induced response can become highly non-linear, espe-  
 269 cially in the  $\beta$  and  $\alpha$  phases. While large photo-induced  
 270 strain is observed across all phases in the large  $n_{ph}$   
 271 regime, Figure 3 and Table II show that the  $\delta$  phase  
 272 possesses the largest photomechanical sensitivity under  
 273 low illumination conditions.

274 A recent study has attributed the large photostriction  
 275 in *cubic* cesium lead halide perovskite to the strong an-  
 276 tibonding nature of the bottom of the conduction band.  
 277 [47] Our results indicate that the strong photo-induced  
 278 strain permeates through all phases of CsPbI<sub>3</sub>, at least in  
 279 the large  $n_{ph}$  regime. The large photo-induced strain in  
 280 CsPbI<sub>3</sub>, and in general in hybrid perovskites [48], may  
 281 find applications in improving the photovoltaic power  
 282 conversion efficiency [49]. Interestingly, to achieve pho-  
 283 tostriction comparable to the 0.125% expansion reported  
 284 in MAPbI<sub>3</sub> films [48], one could use 413 nm wavelength  
 285 laser pulses of 8.5 mJ.cm<sup>-2</sup>.

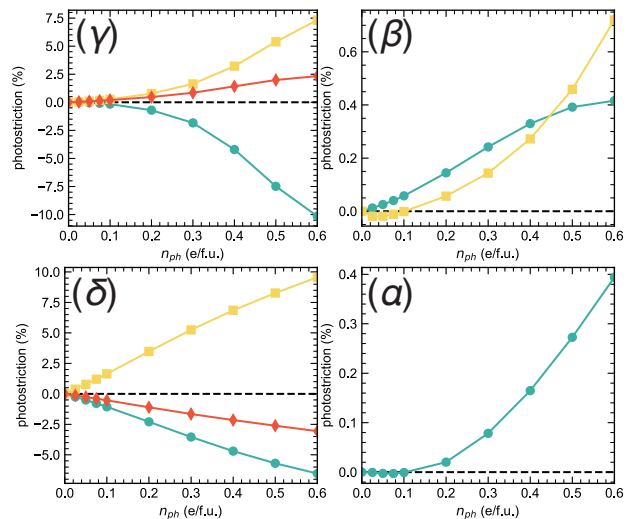


FIG. 3. Photo-induced strain in lead cesium iodide, along the principal crystallographic axes of each phase ( $\gamma$ ), ( $\beta$ ), ( $\delta$ ) and ( $\alpha$ ). Dashed open symbols in the  $\delta$  and  $\gamma$  phases show calculations with SOC.

Material	Phase	$\delta a/a$	$\delta b/b$	$\delta c/c$
% / (e/f.u.)]				
CsPbI <sub>3</sub>	$\alpha$	-0.02	-	-
	$\beta$	0.5	-	-0.8
	$\gamma$	0.2	1.4	1.5
	$\delta$ ,	-9.9	15.3	-5.1
BiFeO <sub>3</sub> (perovskite [44])	$R3c$	-1.5	-	-
BaTiO <sub>3</sub> (perovskite [38])	$R3m$	-0.2	-	-
PbTiO <sub>3</sub> (perovskite [38])	$P4mm$	-1.0	-	-3.1
SrCoO <sub>2.5</sub> (brownmillerite [45])	$Ima2$	-	-	+0.4
SnS (2D ferroelectric [46])		-56.9	14.2-28.4	-

TABLE II. Estimates of the linear photo-induced strain in lead cesium iodide calculated using the constrained-DFT method (no SOC/SOC values reported). Other reported compounds were calculated using the  $\Delta$ SCF (Self-Consistent Field) method.

#### V. CONCLUSION

287 The constrained-DFT approach employed in the  
 288 present study unveils that thermalized photo-excited car-  
 289 riers can reduce, and even invert, the relative energy dif-  
 290 ference between the  $\delta$  phase and the  $\gamma$  perovskite phase  
 291 of CsPbI<sub>3</sub>. This allows to envision new ways to transform  
 292 into or better stabilize the  $\gamma$ -phase, which is highly im-  
 293 portant for photovoltaic applications. In particular, the  
 294 present work proposes that visible light could trigger a  
 295 photo-induced phase transition towards the  $\gamma$  perovskite  
 296 phase, which is of high interest for photovoltaic appli-  
 297 cations. Once the photo-transition is achieved and the  
 298 light removed, it is likely that the  $\gamma$ -phase will remain  
 299 kinetically stable since it has already been proven to be

300 metastable under dark conditions using thermal quench-  
 301 ing [10, 50]. It is unclear at present whether CsPbI<sub>3</sub>  
 302 could sustain the proposed intensity to reach the phase  
 303 transition. Working near the yellow to black phase tran-  
 304 sition temperature should lower the critical value of light  
 305 intensity necessary to reach the transition. Conversely,  
 306 one could expect that using visible illumination (for in-  
 307 stance with lasers) will lower the transition temperature,  
 308 leading to more efficient and ecological manufacturing of  
 309 CsPbI<sub>3</sub>-based devices. In addition, our calculations re-  
 310 veal that CsPbI<sub>3</sub> is an efficient photostrictive material,  
 311 especially in the  $\delta$  phase, which was previously thought  
 312 to be a detrimental phase with respect to photovoltaic  
 313 applications. This work may thus pave the way for other  
 314 and easier applications of CsPbI<sub>3</sub> in photo-actuators.

### 315 ACKNOWLEDGMENTS

316 C. P. acknowledges an international mobility funding  
 317 opportunity from a public grant overseen by the ANR as  
 318 part of the ‘‘Investissements d’Avenir’’ program (ANR-  
 319 10-LABX-0035, LabexNanoSaclay), the Arkansas High  
 320 Performance Computing Center on which calculations  
 321 were performed, and a computing grant from GENCI  
 322 (project AD010913519). L. B. thanks ARO Grant No.  
 323 W911NF-21-1-0113.

### 324 Appendix A: Photo-induced carrier estimate

325 We estimate the photo-excited carrier concentration.  
 326 Considering the power balance sketched in Figure 4, the  
 327 total absorbed energy from a laser of fluence  $I_0$  imping-  
 328 ing on a sample of cross-section  $S$ , thickness  $d$ , having  
 329 absorption and reflection coefficient  $\alpha$  and  $R$  is

$$E_{tot} = (1 - R)I_0(1 - e^{-\alpha d})S \quad (\text{A1})$$

330 As a result, the total number of photons absorbed is

$$N_{photons} = \frac{E_{tot}}{\hbar\omega} = \frac{(1 - R)I_0(1 - e^{-\alpha d})S}{\hbar\omega}, \quad (\text{A2})$$

331 with  $\hbar\omega$  the average photon energy within the incident  
 332 beam. Assuming that each absorbed photon yields an  
 333 electron - hole pair, we would thus have a photo-excited  
 334 carrier density, expressed in e/f.u. of

$$n_{ph} = \frac{N_{photons}}{Sd} \times \frac{V_\delta}{4}, \quad (\text{A3})$$

335 where  $V_\delta$  is the volume of the  $\delta$  phase unit cell. The  
 336 factor 1/4 comes from the fact that there are 4 formula  
 337 units in the  $\delta$  phase unit cell.

338 Assuming, for the sake of simplicity, that photons in  
 339 the laser beam carry an energy  $\hbar\omega = 3$  eV (413 nm), we  
 340 take for the  $\delta$  phase a value of  $\alpha \approx 2 \times 10^5$  cm<sup>-1</sup> [8]. We

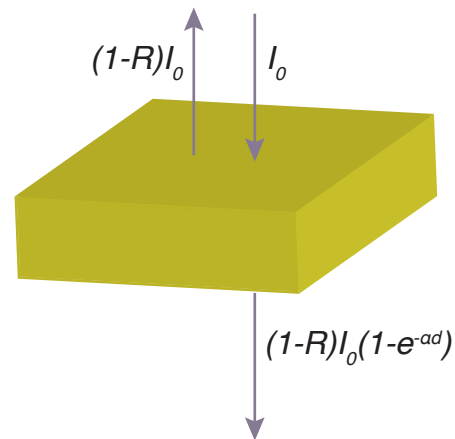


FIG. 4. Sketch of what happens to a ray of light of intensity  $I_0$  impinging on a material.

341 take a reflection coefficient  $R = 0.15$ , similar to what can  
 342 be found in CsPbBr<sub>3</sub> thin films, a parent compound [51].  
 343 This allows us to obtain a crude estimate of the value  
 344 of  $n_{ph}$  depending on the pump fluence, which we plot  
 345 in Figure 5. Note that in Figure 5, we assumed a sam-  
 346 ple uniformly illuminated of thickness 323 nm, area size  
 347  $S = 0.0625$  cm<sup>2</sup>, which is submitted to a laser pulse car-  
 348 rying an energy up to 4 mJ. The geometrical parameters  
 349 involved were taken from photostriction experiments car-  
 350 ried out on thin films of MAPbI<sub>3</sub> [35]. One observes that  
 351 reasonable pulse energy can lead to the desired concen-  
 352 tration of photo-excited carriers in thin films.

353 Note that in the previous simple derivations, we as-  
 354 sumed that every electron-hole pair relaxes into thermal-  
 355 ized carriers in their respective bands (valence bands for  
 356 holes; conduction bands for electrons). We also assume  
 357 that the recombination time of excited carriers is large  
 358 enough compared to the pulse duration. Typical relax-  
 359 ation times in CsPbI<sub>3</sub> are of the order of a few nanosec-  
 360 onds [52, 53] (depending on the sample quality). Picosec-  
 361 ond laser pulses could therefore be suitable this model.  
 362 A more complex model would solve a balance equation or  
 363 the real time Bethe-Salpeter equation to obtain a more  
 364 accurate relation between the pump fluence and the av-  
 365 erage number of photoexcited carriers.

### 366 Appendix B: Numerical integration and toy model

367 One can understand the physical mechanisms at play  
 368 using a simple toy model. It is detailed in Eq. 1. This  
 369 amounts to consider completely flat conduction and val-  
 370 lence bands, *i.e.* a two level system. To further re-  
 371 fine our model, we performed a numerical integration  
 372 of the ground state band structures. In other words,  
 373 we consider a model (denoted as ‘‘ $k$ -sum in the main  
 374 manuscript) of the form:

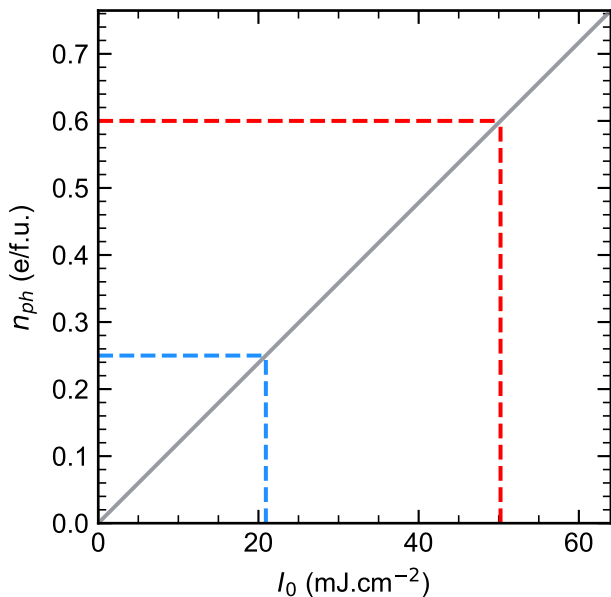


FIG. 5. Estimated photo-induced carrier concentration induced by a 3 eV laser pulse. Dotted blue and red line correspond to the concentration necessary to achieve the  $\delta \rightarrow \gamma$  transition with and without SOC, according to Figure 2 of the main manuscript.

$$E_{\gamma}(n_{ph}) - E_{\delta}(n_{ph}) = \Delta E_0 + [(E_c^{\gamma}(n_{ph}) - E_v^{\gamma}(n_{ph})) - (E_c^{\delta}(n_{ph}) - E_v^{\delta}(n_{ph}))]. \quad (B1)$$

$E_{\gamma/\delta}^c(n_{ph})$  represents the electronic energy change due to the electrons in the conduction band, and can be expressed as:

$$E_c^{\gamma/\delta}(n_{ph}) = \sum_k \sum_c w_k f(\varepsilon_{k,c}^{\gamma/\delta}, \mu_e, T) \varepsilon_{k,c}^{\gamma/\delta}, \quad (B2)$$

where  $c$  represent the conduction band index,  $k$  the  $k$ -point in the irreducible discretized Brillouin zone,  $w_k$  its weight,  $\mu_e$  the electronic quasi-Fermi level,  $T$  the smearing temperature, and  $\varepsilon_{k,c}^{\gamma/\delta}$  is the eigenvalue of  $k$ -point  $k$  with band index  $c$ , taken in the  $\gamma/\delta$  phase calculated with  $n_{ph} = 0$  e/f.u.  $f(\varepsilon_{k,c}^{\gamma/\delta}, \mu_e, T)$  represents the Fermi-Dirac population of this state with energy  $\varepsilon_{k,c}^{\gamma/\delta}$ .

Similarly,  $E_{\gamma/\delta}^v(n_{ph})$  is the energy change caused by the presence of holes in the valence bands.

- [1] J. Jeong, M. Kim, J. Seo, H. Lu, P. Ahlawat, A. Mishra, Y. Yang, M. A. Hope, F. T. Eickemeyer, M. Kim, Y. J. Yoon, I. W. Choi, B. P. Darwich, S. J. Choi, Y. Jo, J. H. Lee, B. Walker, S. M. Zakeeruddin, L. Emsley, U. Rothlisberger, A. Hagfeldt, D. S. Kim, M. Grätzel, and J. Y. Kim, Pseudo-halide anion engineering for  $\alpha$ -FAPbI<sub>3</sub> perovskite solar cells, *Nature* **592**, 381 (2021).
- [2] L. Protesescu, S. Yakunin, M. I. Bodnarchuk, F. Krieg, R. Caputo, C. H. Hendon, R. X. Yang, A. Walsh, and M. V. Kovalenko, Nanocrystals of Cesium Lead Halide Perovskites (CsPbX<sub>3</sub>, X = Cl, Br, and I): Novel Optoelectronic Materials Showing Bright Emission with Wide Color Gamut, *Nano Letters* **15**, 3692 (2015).
- [3] F. Liu, Y. Zhang, C. Ding, S. Kobayashi, T. Izuishi, N. Nakazawa, T. Toyoda, T. Ohta, S. Hayase, T. Minemoto, K. Yoshino, S. Dai, and Q. Shen, Highly luminescent phase-stable cspb<sub>3</sub> perovskite quantum dots achieving near 100% absolute photoluminescence quantum yield, *ACS Nano* **11**, 10373 (2017).
- [4] S.-T. Ha, R. Su, J. Xing, Q. Zhang, and Q. Xiong, Metal halide perovskite nanomaterials: synthesis and applications, *Chemical Science* **8**, 2522 (2017).
- [5] L. Chouhan, S. Ghimire, C. Subrahmanyam, T. Miyasaka, and V. Biju, Synthesis, optoelectronic properties and applications of halide perovskites, *Chemical Society Reviews* **49**, 2869 (2020).
- [6] A. Senocrate, G. Y. Kim, M. Grätzel, and J. Maier, Thermochemical Stability of Hybrid Halide Perovskites, *ACS Energy Letters* **4**, 2859 (2019).
- [7] W. Xiang, S. F. Liu, and W. Tress, A review on the stability of inorganic metal halide perovskites: challenges and opportunities for stable solar cells, *Energy & Environmental Science* **14**, 2090 (2021).
- [8] S. Valastro, G. Mannino, E. Smecca, S. Sanzaro, I. Deretzi, A. L. Magna, A. K. Jena, T. Miyasaka, and A. Alberti, Optical behaviour of  $\gamma$ -black CsPbI<sub>3</sub> phases formed by quenching from 80 °C and 325 °C, *JPhys Materials* **4**, 10.1088/2515-7639/abfa7a (2021).
- [9] D. B. Straus, S. Guo, A. M. Abeykoon, and R. J. Cava, Understanding the Instability of the Halide Perovskite CsPbI<sub>3</sub> through Temperature-Dependent Structural Analysis, *Advanced Materials* **32**, 1 (2020).
- [10] J. A. Steele, H. Jin, I. Dovgaliuk, R. F. Berger, T. Braeckevelt, H. Yuan, C. Martin, E. Solano, K. Lejaeghere, S. M. J. Rogge, C. Notebaert, W. Vandezande, K. P. F. Janssen, B. Goderis, E. Debroye, Y.-K. Wang, Y. Dong, D. Ma, M. Saidaminov, H. Tan, Z. Lu, V. Dyadkin, D. Chernyshov, V. Van Speybroeck, E. H. Sargent, J. Hofkens, and M. B. J. Roeffaers, Thermal nonequilibrium of strained black CsPbI<sub>3</sub> thin films, *Science* **365**, 679 (2019).
- [11] A. Jain, S. P. Ong, G. Hautier, W. Chen, W. D. Richards, S. Dacek, S. Cholia, D. Gunter, D. Skinner, G. Ceder, and K. a. Persson, The Materials Project: A materials genome approach to accelerating materials innovation, *APL Materials* **1**, 011002 (2013).
- [12] B. Kundys, Photostrictive materials, *Applied Physics Reviews* **2**, 011301 (2015).

- [13] C. Paillard, E. Torun, L. Wirtz, J. Íñiguez, and L. Bellaiche, Photoinduced Phase Transitions in Ferroelectrics, *Physical Review Letters* **123**, 087601 (2019).
- [14] X. Gonze, B. Amadon, G. Antonius, F. Arnardi, L. Baguet, J.-M. Beuken, J. Bieder, F. Bottin, J. Bouchet, E. Bousquet, N. Brouwer, F. Bruneval, G. Brunin, T. Cavignac, J.-B. Charraud, W. Chen, M. Côté, S. Cottenier, J. Denier, G. Geneste, P. Ghosez, M. Giantomassi, Y. Gillet, O. Gingras, D. R. Hamann, G. Hautier, X. He, N. Helbig, N. Holzwarth, Y. Jia, F. Jollet, W. Lafargue-Dit-Hauret, K. Lejaeghere, M. A. Marques, A. Martin, C. Martins, H. P. Miranda, F. Naccarato, K. Persson, G. Petretto, V. Planes, Y. Pouillon, S. Prokhorenko, F. Ricci, G.-M. Rignanese, A. H. Romero, M. M. Schmitt, M. Torrent, M. J. van Setten, B. Van Troeye, M. J. Verstraete, G. Zérah, and J. W. Zwanziger, The Abinit project: Impact, environment and recent developments, *Computer Physics Communications* **248**, 107042 (2020).
- [15] A. H. Romero, D. C. Allan, B. Amadon, G. Antonius, T. Applencourt, L. Baguet, J. Bieder, F. Bottin, J. Bouchet, E. Bousquet, F. Bruneval, G. Brunin, D. Caliste, M. Côté, J. Denier, C. Dreyer, P. Ghosez, M. Giantomassi, Y. Gillet, O. Gingras, D. R. Hamann, G. Hautier, F. Jollet, G. Jomard, A. Martin, H. P. C. Miranda, F. Naccarato, G. Petretto, N. A. Pike, V. Planes, S. Prokhorenko, T. Rangel, F. Ricci, G.-M. Rignanese, M. Royo, M. Stengel, M. Torrent, M. J. van Setten, B. V. Troeye, M. J. Verstraete, J. Wiktor, J. W. Zwanziger, and X. Gonze, Abinit: Overview, and focus on selected capabilities, *J. Chem. Phys.* **152**, 124102 (2020).
- [16] X. Gonze, F. Jollet, F. Abreu Araujo, D. Adams, B. Amadon, T. Applencourt, C. Audouze, J.-M. Beuken, J. Bieder, A. Bokhanchuk, E. Bousquet, F. Bruneval, D. Caliste, M. Côté, F. Dahm, F. Da Pieve, M. Delaveau, M. Di Gennaro, B. Dorado, C. Espejo, G. Geneste, L. Genovese, A. Gerossier, M. Giantomassi, Y. Gillet, D. Hamann, L. He, G. Jomard, J. Laflamme Janssen, S. Le Roux, A. Levitt, A. Lherbier, F. Liu, I. Lukačević, A. Martin, C. Martins, M. Oliveira, S. Poncé, Y. Pouillon, T. Rangel, G.-M. Rignanese, A. Romero, B. Rousseau, O. Rubel, A. Shukri, M. Stankovski, M. Torrent, M. Van Setten, B. Van Troeye, M. Verstraete, D. Waroquiers, J. Wiktor, B. Xu, A. Zhou, and J. Zwanziger, Recent developments in the ABINIT software package, *Computer Physics Communications* **205**, 106 (2016).
- [17] M. Torrent, F. Jollet, F. Bottin, G. Zérah, and X. Gonze, Implementation of the projector augmented-wave method in the ABINIT code: Application to the study of iron under pressure, *Computational Materials Science* **42**, 337 (2008).
- [18] F. Bottin, S. Leroux, A. Knyazev, and G. Zérah, Large-scale ab initio calculations based on three levels of parallelization, *Computational Materials Science* **42**, 329 (2008).
- [19] F. Jollet, M. Torrent, and N. Holzwarth, Generation of Projector Augmented-Wave atomic data: A 71 element validated table in the XML format, *Computer Physics Communications* **185**, 1246 (2014).
- [20] JTH -v1.1 table (2021).
- [21] N. Holzwarth, A. Tackett, and G. Matthews, A Projector Augmented Wave (PAW) code for electronic structure calculations, Part I: atompaw for generating atom-centered functions, *Computer Physics Communications* **135**, 329 (2001).
- [22] A. Marrognier, G. Roma, S. Boyer-Richard, L. Pedesseau, J.-M. Jancu, Y. Bonnassieux, C. Katan, C. C. Stoumpos, M. G. Kanatzidis, and J. Even, Anharmonicity and Disorder in the Black Phases of Cesium Lead Iodide Used for Stable Inorganic Perovskite Solar Cells, *ACS Nano* **12**, 3477 (2018).
- [23] D. Liu, Z. Shao, C. Li, S. Pang, Y. Yan, and G. Cui, Structural Properties and Stability of Inorganic CsPbI<sub>3</sub> Perovskites, *Small Structures* **2**, 2000089 (2021).
- [24] See supplementary information at <https://www. ...com>, where crystallographic structures, comparison of SOC and no SOC calculations and phonon instabilities in the cubic perovskite phase are presented. (2021).
- [25] W. Setyawan and S. Curtarolo, High-throughput electronic band structure calculations: Challenges and tools, *Computational Materials Science* **49**, 299 (2010), arXiv:1004.2974.
- [26] J. Even, L. Pedesseau, J.-M. Jancu, and C. Katan, Importance of Spin-Orbit Coupling in Hybrid Organic-Inorganic Perovskites for Photovoltaic Applications, *The Journal of Physical Chemistry Letters* **4**, 2999 (2013).
- [27] J. Brgoch, A. J. Lehner, M. Chabinyč, and R. Seshadri, Ab Initio Calculations of Band Gaps and Absolute Band Positions of Polymorphs of RbPbI<sub>3</sub> and CsPbI<sub>3</sub>: Implications for Main-Group Halide Perovskite Photovoltaics, *The Journal of Physical Chemistry C* **118**, 27721 (2014).
- [28] M. A. Fadla, B. Bentría, T. Dahame, and A. Benghia, First-principles investigation on the stability and material properties of all-inorganic cesium lead iodide perovskites CsPbI<sub>3</sub> polymorphs, *Physica B: Condensed Matter* **585**, 412118 (2020).
- [29] L.-K. Gao and Y.-L. Tang, Theoretical Study on the Carrier Mobility and Optical Properties of CsPbI<sub>3</sub> by DFT, *ACS Omega* **6**, 11545 (2021).
- [30] I. Deretzis, C. Bongiorno, G. Mannino, E. Smecca, S. Sanzaro, S. Valastro, G. Fiscaro, A. La Magna, and A. Alberti, Exploring the Structural Competition between the Black and the Yellow Phase of CsPbI<sub>3</sub>, *Nanomaterials* **11**, 1282 (2021).
- [31] S. Xu, A. Libanori, G. Luo, and J. Chen, Engineering bandgap of CsPbI<sub>3</sub> over 1.7 eV with enhanced stability and transport properties, *iScience* **24**, 102235 (2021).
- [32] J.-C. Tung, Y.-H. Hsieh, and P.-L. Liu, Strain Induced Topological Insulator Phase in CsPbBr<sub>3</sub>I<sub>1-x</sub> (x = 0, 1, 2, and 3) Perovskite: A Theoretical Study, *Applied Sciences* **11**, 5353 (2021).
- [33] R. J. Sutton, M. R. Filip, A. A. Haghighirad, N. Sakai, B. Wenger, F. Giustino, and H. J. Snaith, Cubic or Orthorhombic? Revealing the Crystal Structure of Metastable Black-Phase CsPbI<sub>3</sub> by Theory and Experiment, *ACS Energy Letters* **3**, 1787 (2018).
- [34] H. Yao, J. Zhao, Z. Li, Z. Ci, and Z. Jin, Research and progress of black metastable phase CsPbI<sub>3</sub> solar cells, *Materials Chemistry Frontiers* **5**, 1221 (2021).
- [35] X. Du, J. Li, G. Niu, J.-H. Yuan, K. -H. Xue, M. Xia, W. Pan, X. Yang, B. Zhu, and J. Tang, Lead halide perovskite for efficient optoacoustic conversion and application toward high-resolution ultrasound imaging, *Nat. Comm.* **12**, 3348 (2021).
- [36] B. Peng, Y. Hu, S. Murakami, T. Zhang, and B. Monserat, Topological phonons in oxide perovskites con-

- 573 trolled by light, *Science Advances* **6**, eabd1618 (2020),  
574 arXiv:2011.06269.
- 575 [37] R. E. Pasynkov, On some problems of the phenomenolog-  
576 ical theory of ferroelectric-semiconductors, *Ferroelectrics*  
577 **6**, 19 (1973).
- 578 [38] C. Paillard, S. Prosandeev, and L. Bellaiche, Ab initio  
579 approach to photostriction in classical ferroelectric ma-  
580 terials, *Physical Review B* **96**, 045205 (2017)  
581 .
- 582 [39] Z. Yang, A. Surrente, K. Galkowski, A. Miyata, O. Por-  
583 tugall, R. J. Sutton, A. A. Haghighirad, H. J. Snaith,  
584 D. K. Maude, P. Plochocka, and R. J. Nicholas, Impact  
585 of the Halide Cage on the Electronic Properties of Fully  
586 Inorganic Cesium Lead Halide Perovskites, *ACS Energy*  
587 *Letters* **2**, 1621 (2017), arXiv:1706.04489.
- 588 [40] P. Basera, A. Singh, D. Gill, and S. Bhattacharya,  
589 Capturing Excitonic Effects in Lead Iodide Perovskites  
590 from Many-Body Perturbation Theory, (2020),  
591 arXiv:2008.03381.
- 592 [41] M. R. Filip, J. B. Haber, and J. B. Neaton, Phonon  
593 Screening of Excitons in Semiconductors: Halide Perovskites  
594 and Beyond, *Physical Review Letters* **127**,  
595 067401 (2021), arXiv:2106.08697.
- 596 [42] X. G. Zhao, G. M. Dalpian, Z. Wang, and A. Zunger,  
597 Polymorphous nature of cubic halide perovskites, *Physical*  
598 *Review B* **101**, 155137 (2020), arXiv:1905.09141.
- 599 [43] X. Wang, K. Patel, S. Prosandeev, Y. Zhang, C. Zhong,  
600 B. Xu, and L. Bellaiche, Finite-Temperature Dynamics in  
601 Cesium Lead Iodide Halide Perovskite, *Advanced Func-*  
602 *tional Materials* **2106264**, 2106264 (2021).
- 603 [44] C. Paillard, B. Xu, B. Dkhil, G. Geneste, and L. Bel-  
604 laiche, Photostriction in Ferroelectrics from Density  
605 Functional Theory, *Physical Review Letters* **116**, 247401  
606 (2016).
- 607 [45] B. Zhang, X. He, J. Zhao, C. Yu, H. Wen, S. Meng,  
608 E. Bousquet, Y. Li, C. Ge, K. Jin, Y. Tao, and  
609 H. Guo, Giant photoinduced lattice distortion in oxygen  
610 vacancy ordered  $\text{A}_{1-x}\text{B}_x\text{SrCoO}_{3-y}$  thin  
611 films, *Physical Review B* **100**, 144201 (2019).
- 613 [46] R. Haleoot, C. Paillard, T. P. Kaloni, M. Mehboudi,  
614 B. Xu, L. Bellaiche, and S. Barraza-Lopez, Photostrictive  
615 Two-Dimensional Materials in the Monochalcogenide  
616 Family, *Physical Review Letters* **118**, 227401 (2017),  
617 arXiv:1701.02249.
- 618 [47] B. Peng, D. Bennett, I. Bravić, and B. Monserrat, Tun-  
619 able Photostriction of Halide Perovskites through En-  
620 ergy Dependent Photoexcitation, *Phys. Rev. Mater.* **6**,  
621 L082401 (2022).
- 622 [48] Y. Zhou, L. You, S. Wang, Z. Ku, H. Fan, D. Schmidt,  
623 A. Rusydi, L. Chang, L. Wang, P. Ren, L. Chen,  
624 G. Yuan, L. Chen, and J. Wang, Giant photostriction in  
625 organic-inorganic lead halide perovskites, *Nature Com-*  
626 *munications* **7**, 11193 (2016).
- 627 [49] H. Tsai, R. Asadpour, J.-C. Blancon, C. C. Stoumpos,  
628 O. Durand, J. W. Strzalka, B. Chen, R. Verduzco,  
629 P. M. Ajayan, S. Tretiak, J. Even, M. A. Alam, M. G.  
630 Kanatzidis, W. Nie, and A. D. Mohite, Light-induced  
631 lattice expansion leads to high-efficiency perovskite solar  
632 cells, *Science* **360**, 67 (2018)  
633 .
- 634 [50] G. E. Eperon, G. M. Paternò, R. J. Sutton, A. Zam-  
635 petti, A. A. Haghighirad, F. Cacialli, and H. J. Snaith,  
636 Inorganic Caesium Lead Iodide Perovskite Solar Cells, *J.*  
637 *Mater. Chem. A* **3**, 19688 (2015).
- 638 [51] W. Yan, L. Mao, P. Zhao, A. Mertens, S. Dottermusch,  
639 H. Hu, Z. Jin, and B. S. Richards, Determination of com-  
640 plex optical constants and photovoltaic device design of  
641 all-inorganic CsPbBr<sub>3</sub> perovskite thin films, *Optics Ex-*  
642 *press* **28**, 15706 (2020).
- 643 [52] S. Dastidar, S. Li, S. Y. Smolin, J. B. Baxter, and A. T.  
644 Fafarman, Slow Electron-Hole Recombination in Lead  
645 Iodide Perovskites Does Not Require a Molecular Dipole,  
646 *ACS Energy Letters* **2**, 2239 (2017).
- 647 [53] C. de Weerd, L. Gomez, A. Capretti, D. M. Lebrun,  
648 E. Matsubara, J. Lin, M. Ashida, F. C. Spoor, L. D.  
649 Siebbeles, A. J. Houtepen, K. Suenaga, Y. Fujiwara,  
650 and T. Gregorkiewicz, Efficient carrier multiplication  
651 in CsPbI<sub>3</sub> perovskite nanocrystals, *Nature Communica-*  
652 *tions* **9**, 1 (2018)